Band-gap engineering and ballistic transport in edge-corrugated graphene nanoribbons

S. Ihnatsenka,[1] I. V. Zozoulenko,[2] and G. Kirczenow[1]
[1]*Department of Physics, Simon Fraser University, Burnaby, British Columbia, Canada V5A 1S6*
[2]*Solid State Electronics, ITN, Linköping University, 601 74 Norrköping, Sweden*
(Received 10 June 2009; revised manuscript received 14 August 2009; published 5 October 2009)

We calculate the band structure and the conductance of periodic edge-corrugated graphene nanoribbons within the framework of the tight-binding *p*-orbital model. We consider corrugated structures based on host ribbons with armchair and zigzag edges and three different types of corrugations (armchair edges, zigzag edges, as well as a rectangular corrugation). We demonstrate that for armchair host ribbons, depending on the type of corrugation, a band gap or low-velocity minibands appear near the charge neutrality point. For higher energies the allowed Bloch state bands become separated by ministopbands. By contrast, for corrugated ribbons with the zigzag host, the corrugations introduce neither band gaps nor stopbands (except for the case of the rectangular corrugations). The conductances of finite edge-corrugated ribbons are analyzed on the basis of the corresponding band structures. For a sufficiently large number of corrugations the conductance follows the number of the corresponding propagating Bloch states and shows pronounced oscillations due to the Fabry-Perot interference within the corrugated segments. Finally we demonstrate that edge disorder strongly affects the conductances of corrugated ribbons. Our results indicate that observation of miniband formation in corrugated ribbons would require clean, edge-disorder free samples, especially for the case of the armchair host lattice.

DOI: 10.1103/PhysRevB.80.155415 PACS number(s): 73.23.Ad, 73.63.Bd, 73.22.Dj

I. INTRODUCTION

One of the most fascinating recent discoveries in condensed-matter physics is the fabrication and demonstration of electrical conductance in graphene—a single sheet of carbon atoms arranged in a honeycomb lattice.[1] This discovery has ignited a tremendous interest of the research community not only because of the new exciting physics that the graphene exhibits but also because of the promise of graphene-based high-speed electronics.[2]

While earlier works on graphene have been focused on bulk samples, recent studies have also addressed material, electronic, and transport properties of *confined* structures such as nanoribons,[3–5] nanoconstrictions,[6] quantum dots,[7–9] and antidots.[10] The confinement and the patterning of graphene with few nanometer precision is typically achieved by means of electron-beam lithography and etching techniques. Particular attention has been paid to the control of morphology, geometry, and stability of the device edges.[11,12] These advances in graphene material technology and device processing make it possible to fabricate ballistic periodic graphene structures with nanometer feature sizes.

Periodic quasi-one-dimensional (quasi-1D) systems defined in conventional two-dimensional electron-gas (2DEG) heterostructures such as corrugated channels,[13–15] ballistic one-dimensional superlattices,[16] and arrays of quantum dots[17] and antidots[18,19] have been the subject of intense research during the past 20 years. These artificial finite crystal structures show a wealth of phenomena related to the formation of miniband structure and quantum interference. Recently, a periodic structure defined in graphene, an antidot lattice, has been studied theoretically by Pedersen *et al.*[20] They demonstrated that the antidot lattice can turn semimetallic graphene into a gapped semiconductor, where the size of the gap can be tuned via the geometry of the lattice. An experimental realization of the antidot array has been recently reported by Shen *et al.*[10] who observed the commensurability oscillations and Aharonov-Bohm oscillations arising from the artificially imposed lateral potential modulation. Electronic properties of another periodic structure, sawtoothlike graphene nanoribbons, have been recently studied by Wu and Zeng[21] who demonstrated that the unique edge structures of the sawtoothlike ribbons induce richer band-gap features than its straight counterpart.

Motivated by these advances in devices processing and fabrication, in the present paper we address the electronic and transport properties of periodic edge-corrugated ballistic nanoribbons. The ballistic nanoribbons represent the fundamental building blocks of graphene-based nanocircuits and/or individual devices. Understanding the factors that affect the electronic and transport properties of graphene nanoribbons and exploring ways to control these properties through periodic corrugations are the central aims of our study.

The paper is organized as follows. In Sec. II we present a model of corrugated graphene nanoribbons and briefly outline the basics of our calculations of the band structure, Bloch states, and the conductance based on the recursive Green's function technique. In Sec. III we calculate the band structures of zigzag and armchair nanoribbons with different corrugations and discuss formation/suppression of the band gap as well as the formation of stopbands. We calculate the conductances of finite corrugated nanoribbons and discuss them on the basis of the corresponding band structures. Finally, we address the effect of the edge disorder on the conductances of realistic corrugated nanoribbons. The main conclusions of our study are presented in Sec. IV.

II. MODEL

We describe a graphene ribbon by the standard tight-binding Hamiltonian on a honeycomb lattice,

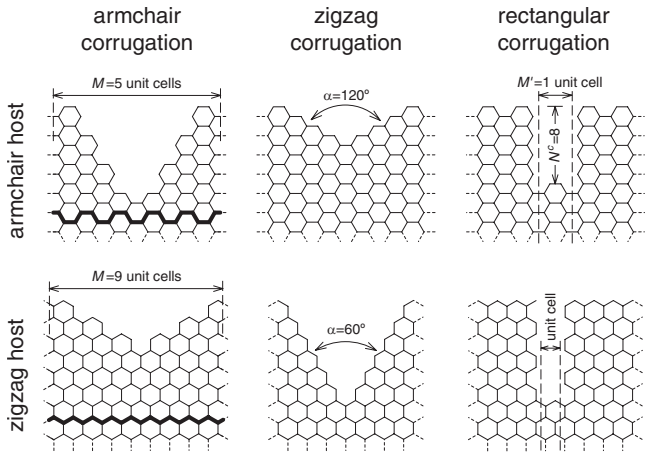

FIG. 1. Schematic representation of corrugations studied in the present paper. M is the corrugation unit cell. M' and N^c are the length and depth of a rectangular groove.

$$H = \sum_i \epsilon_i a_i^\dagger a_i - \sum_{\langle i,j \rangle} t_{ij}(a_i^\dagger a_j + \text{H.c.}), \tag{1}$$

where ϵ_i is the on-site energy, $\epsilon_i=0$ in the following, and $t_{ij}=t=2.7$ eV is the overlap integral between nearest-neighbor atoms. This Hamiltonian is appropriate for graphene with one dangling p_z orbital per carbon atom and is known to describe the π band dispersion well at low energies.[22] Spin and electron interaction effects are outside of the scope of our study. We also disregard the effect of modification of the hopping integrals close to the ribbon edges as we have verified that this modification has a negligible effect on the electronic structure of the relatively wide ribbons studied in this work. The effects of corrugations are incorporated by removing carbon atoms and setting appropriate hopping elements t_{ij} to zero. It is assumed that atoms at the edges are attached to two other carbon atoms and passivated by a neutral chemical ligand, such as hydrogen. There are two especially simple classes of corrugations: those with armchair edges and those with zigzag edges. Depending on the edge type and orientation of the host ribbon, an apex angle will equal $\alpha=60°$ or 120°, see Fig. 1 and the insets in Figs. 2 and 4. For a given edge, host and α, it is possible to change the corrugation size by varying its length M. As M becomes longer the groove penetrates deeper into the host material until only a single carbon-carbon link persists in the constriction. As a motivation for this choice of corrugation we refer to the recent studies[11,12] demonstrating controlled edge reconstruction with the formation of the sharp stabilized zigzag or armchair edges. For the sake of completeness, we consider also a third corrugation type, which has a rectangular shape. Its distinctive feature is the presence of zigzag (armchair) edges joining the armchair (zigzag) edges of the wide and narrow regions.

The Bloch states of the corrugated ribbons are calculated using the Green's function technique.[23] We consider infinitely long graphene ribbons with imposed periodic corrugation in the longitudinal direction. For a translationally invariant system, the solutions of the Schrodinger equation with Hamiltonian (1) obey the Bloch theorem,

$$\Psi_{m+M} = e^{ikM}\Psi_m, \tag{2}$$

where k is the Bloch wave vector and Ψ_m is the Bloch wave function at coordinate m. Introducing the Green's function $G=(E-H)^{-1}$ and using Eq. (2), we formulated the eigenproblem as stated in Ref. 23 and then solved it numerically. Knowledge of the Bloch states allows one to construct the band diagram, which in turn serves as a basis for analysis of

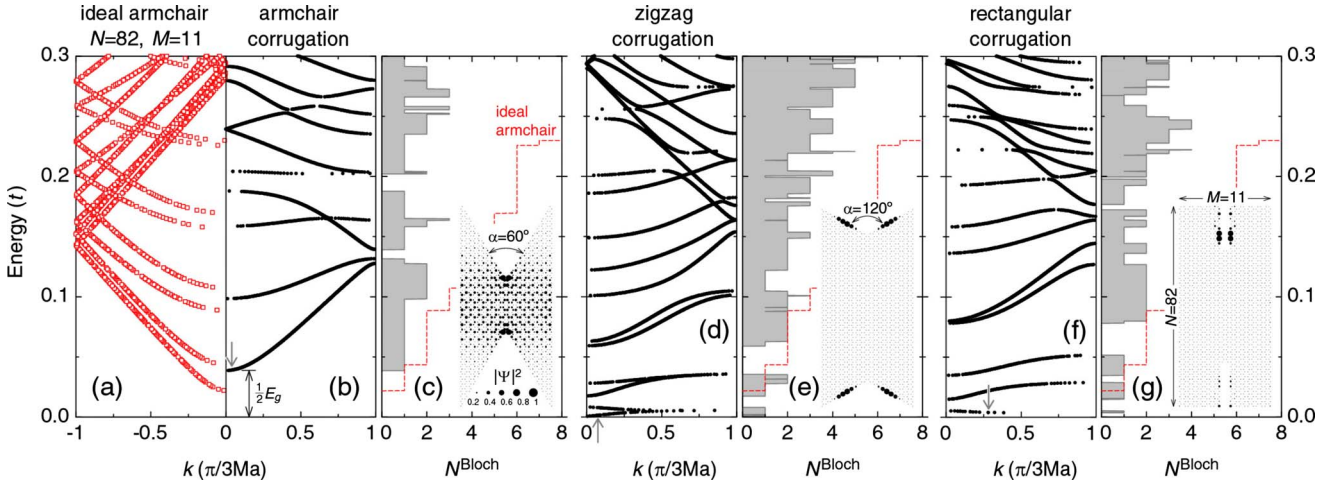

FIG. 2. (Color online) (a) Band structure of ideal and [(b), (d), and (g)] corrugated graphene ribbons with the armchair host. The ideal band structure in (a) has been zone folded for easier comparison with (b), (d), and (f). The band gap E_g is increased if a corrugation with armchair edges is imposed (b). However low-energy minibands appear if zigzag edges are present in the corrugation (d) and (f). They are associated with electron localization along the zigzag edges as shown in the insets in (e) and (g); the wave-function modulus $|\Psi|^2$ is given for k vectors marked by arrows. The plots (c), (e), and (g) show the number of the propagating Bloch states N^{Bloch}: the dashed line corresponds to the ideal ribbon while the gray solid curve with the filled area presents the corrugated case. The host ribbon has $N=82$ carbon atoms in the transverse direction (~10 nm width) and $M=11$ unit cells in the longitudinal direction. $t=2.7$ eV and $a=0.142$ nm.

transport properties of the periodically corrugated graphene ribbons.

To analyze the transport properties, we consider n periodically repeated corrugations attached to ideal semi-infinite leads. The semi-infinite leads consist of graphene ribbons with the same edge orientation as the host orientation of the corrugated region. As the number of corrugations increases, $n \gg 1$, we may expect the transport properties of the corrugated channel to be governed by the Bloch states.[14,19] In the opposite limit of $n=1$, the transport is determined by scattering and localization at the edges of a single constriction.[24]

The central quantity in transport calculations is the conductance. In the linear-response regime for zero temperature, it is given by the Landauer formula

$$G = \frac{2e^2}{h} T, \tag{3}$$

with T being the total transmission coefficient. The transmission coefficient is calculated by the recursive Green's function method, see Ref. 23 for details. Note that knowledge of the Green's function allows one also to obtain other useful information such as wave functions, density of states, and currents.[23,25]

III. RESULTS AND DISCUSSION

Figures 2(b), 2(d), and 2(f) show representative band structures of infinite periodic graphene ribbons with different types of corrugations. All of them are created from the armchair host of $N=82$ carbon atom width and $M=11$ unit-cell length. These sizes correspond approximately to 10 nm width and 5 nm length. For reference purposes, Fig. 2(a) presents the band structure of the ideal host armchair ribbon. It has a band gap of $E_g=0.042t$ as expected for $N=82$.[26,27] When the corrugation is imposed, the band diagram undergoes substantial changes. First, for the case of the corrugation with the armchair edge the band gap substantially changes (in the case under consideration it increases by a factor of 1.8), Fig. 2(b). However, for the zigzag edge corrugation, conductive minibands appear near the charge neutrality point $E=0$, Figs. 2(d) and 2(f). These minibands are very flat indicating their low velocity. Inspection of the wave functions demonstrates that electrons in the low lying minibands are strongly localized to the zigzag edges. Second, different bands of Bloch states become separated by gaps or so-called ministopbands.[28] Their nature is related to the Bragg reflection due to the periodic perturbation.[13,14,16,29] Third, the number of propagating Bloch states decreases at most energies in comparison to the ideal ribbon, Figs. 2(c), 2(e), and 2(g). Fourth, in many cases avoided crossings of different minibands result in abrupt drops in the number of propagating states in narrow ranges of energy. Note that for most energies the number of Bloch states, N^{Bloch}, is smaller for corrugated channels than for the corresponding ideal nanoribbons. However, for the armchair host ribbons in certain energy intervals N^{Bloch} for these corrugated ribbons exceeds the corresponding number of propagating states for the ideal ribbons. This is explained by the fact that because of the presence of the zigzag corrugation the corrugated armchair host structure acquires certain properties of the zigzag ribbons. In particular, the corrugated ribbon can support edge states of the kind that exist in zigzag ribbons but which are absent in the armchair host channel [for illustration of the edge state that exist in the energy gap of the corresponding ideal ribbon see the wave function shown in Fig. 2(e)].

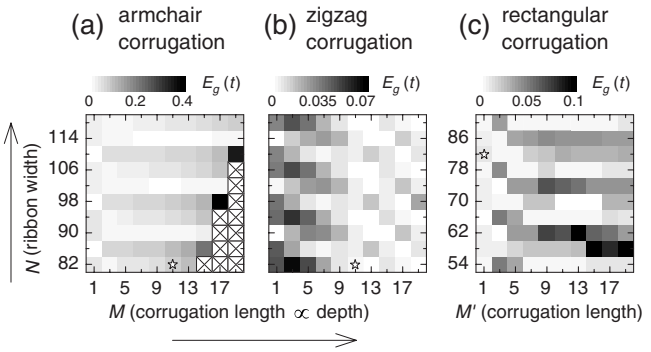

FIG. 3. The band gap E_g vs width N of the host ribbon and length M of the corrugation for the armchair host. Increase in M leads to progressive corrugation deepening and constriction narrowing for both the armchair and zigzag edges of corrugation. Diagonal crosses indicate where the constrictions have been completely closed off. In the case of the rectangular corrugation, its depth is fixed to be $N^c=18$ carbon atoms while the length M' increases [note that M' is the slit width and the length of the unit cell of the corrugation equals M' plus ten unit cells of the host armchair ribbon, see inset in Fig. 2(g)]. Stars mark $N=82$ and $M=11$ setups shown in Fig. 2.

We also performed systematic calculations of the band structures of corrugated ribbons of different width N and periodicity M. While all of them exhibit similar behavior as outlined above for a representative ribbon of $N=82$ and $M=11$, particular features of the band structure depend in a sensitive way on the width of the host ribbon N and the corrugation periodicity M. This is illustrated in Fig. 3 that shows the size of the band gap as a function of the corrugation strength for the armchair host ribbon. In the interval of N considered, the host ribbons of width $N=86,98,110$ are metallic; all other are semiconducting. For the case of the armchair corrugation, E_g gradually increases as the constrictions narrow (i.e., M increases) for most values of N, Fig. 3(a). However, for a sequence $N=90,102,114$ (corresponding to the semiconducting host ribbons), the band gap slowly decreases and remains rather small [this periodic dependence of the E_g on the ribbon width is clearly seen as horizontal trenches in Fig. 3(a)]. This can be explained by the fact that for this sequence the width of the corrugated ribbon in its narrowest part, N_{narr}, shows metallic behavior for all M [i.e., the corresponding uniform ribbon of constant width N_{narr} is metallic;[26,27] note that M is odd in Fig. 3(a)] while for all other N, the minimal width N_{narr} corresponds to the semiconducting behavior. For the case of zigzag corrugation, the dependence of E_g on the corrugation strength M exhibits the opposite trend, Fig. 3(b). We attribute this to the nature of zigzag edges, which favor electron propagation at low energy. Thus for zigzag corrugations the gap tends to be larger for small M, for which the zigzag corrugations are interrupted most often by armchair "defects" that occur at each

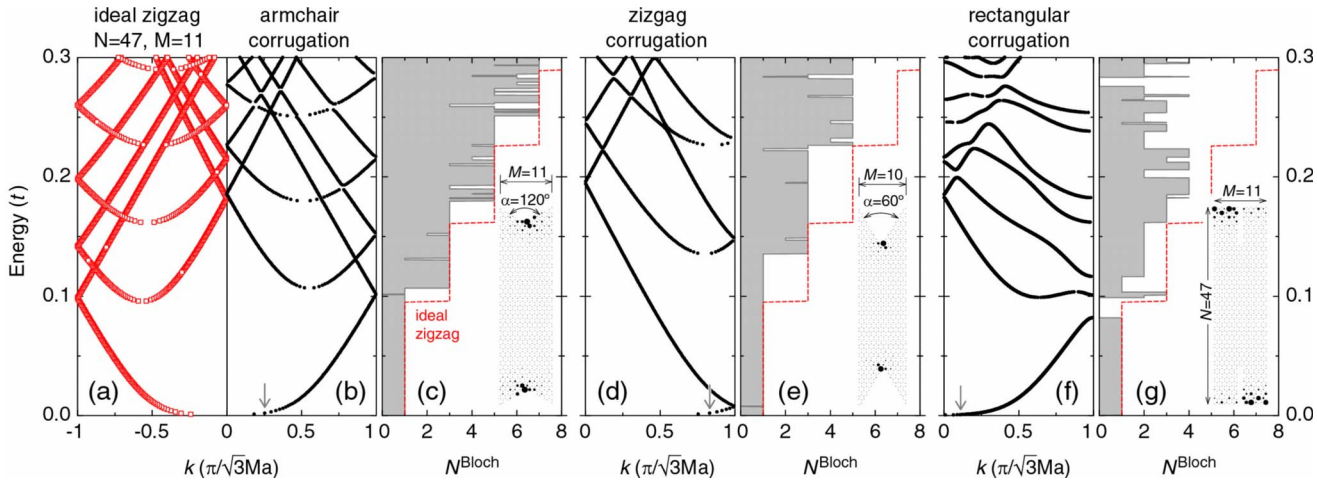

FIG. 4. (Color online) The same as Fig. 2 but for the zigzag host ribbon. The host ribbon has $N=47$ carbon atoms in the transverse direction (~ 10 nm width) and $M=11$ unit cells in the longitudinal direction except (d) and (e) where $M=10$.

apex of the corrugated structure for zigzag corrugation of the armchair host as can be seen in Fig. 1. The rectangular corrugation has many similarities with the armchair case, though electron interference at sharp corners becomes much more important. If the constriction is long enough, substantial band gaps might develop.

Let us now consider the case of the zigzag orientation of the host ribbon, Fig. 4. The zigzag edges of graphene ribbons are known to accommodate exponentially localized edge states.[26] Independent of the width, zigzag ribbons are metallic with a zero band gap. None of the corrugation types changes this feature and the ribbon stays metallic unless the constrictions are a few atoms wide. As the corrugation deepens into host material, the locations where the electron wave functions are localized shift accordingly, see insets in Figs. 4(c) and 4(e). Robust metallic behavior is also related to a peculiar current-density distribution, which is mainly concentrated along the center of the ribbon.[24,30] Substantial ministopbands were found to develop for the rectangular corrugation only, Figs. 4(f) and 4(g). [Though there are extremely narrow stopbands in Figs. 4(b)–4(e), they are two orders of magnitude narrower and thus unlikely to be observed experimentally.] Because of the abrupt change in the edge configurations electrons stay localized near the edges of the wide regions in this case, see inset in Fig. 4(g).

Let us now turn to the transport properties of the corrugated ribbons and the relation to the Bloch states. Figures 5 and 6 show the conductance as a function of the Fermi energy for different number of the corrugations. We build up the central scattering region by connecting the corrugations in series and adding semi-infinite ribbons, that play the role of ideal leads, to both ends. The latter has the same edge orientation as the host of the corrugated part, e.g., they are armchair in Fig. 5 and zigzag in Fig. 6. The most striking feature of these figures is the reduction in the conductance relative to that for the corresponding infinite corrugated ribbons which is given by $\frac{2e^2}{h}N^{\mathrm{Bloch}}$, where N^{Bloch} is the number of Bloch states at the Fermi energy in the infinite corrugated structure. As the number of corrugations grows the conductance follows $\frac{2e^2}{h}N^{\mathrm{Bloch}}$ more closely. The strong oscillations observed in Fig. 5 are caused by the Fabry-Perot interference of electron waves inside the scattering region, see the topmost inset for the wave-function modulus. If the energy of the incident electron falls into the stop miniband the conductance may be suppressed by many orders of magnitude due to destructive interference as is seen at energies near $0.2t$ in the lower panel of Fig. 5. These features in the conductance of the corrugated ribbons are very similar to those of quasi-1D periodic systems defined in conventional 2DEG heterostructures.[13,14,16,19] As is seen in Fig. 6, the electron states existing in the zigzag ribbons have peculiar properties making them relatively immune to the corrugations: the conductance deviates very little from $\frac{2e^2}{h}N^{\mathrm{Bloch}}$. The wave functions effectively round the grooves and enhanced localization of $|\Psi|^2$ becomes pronounced at the apexes, Fig. 6. This behavior resembles somewhat that of the edge states in the quantum Hall regime. The above discussion is for armchair corrugations. The transport properties of ribbons with zigzag and rectangular corrugations relate to the band structures and wave functions of those systems that are discussed above in a similar way.

Note that our single-particle conductance calculations do not account for charging (Coulomb blockade) effects. However, inspection of the wave function in the corrugated ribbons for the zigzag host near the charge neutrality point $E=0$ (and the corresponding Bloch states) indicates that charging effects may dominate the conductance in this regime. Indeed, because of the strong electron localization near its apexes, the corrugated ribbon effectively behaves as an array of weakly coupled quantum dots, see Figs. 4 and 6. This behavior is also reflected in a very low group velocity of the corresponding energy bands. Thus, the corrugated ribbon with the zigzag host is expected to effectively function as an array of weakly coupled quantum dots, even though the corrugations can be relatively small in comparison to the ribbon's width.

It is well known that the disorder inevitably present in realistic devices has a marked effect on the conductance.[4,31] Figure 7 shows representative results for both a corrugated ribbon and the straight ribbon of the same size. The disorder is introduced onto the edges only and the host ribbon and

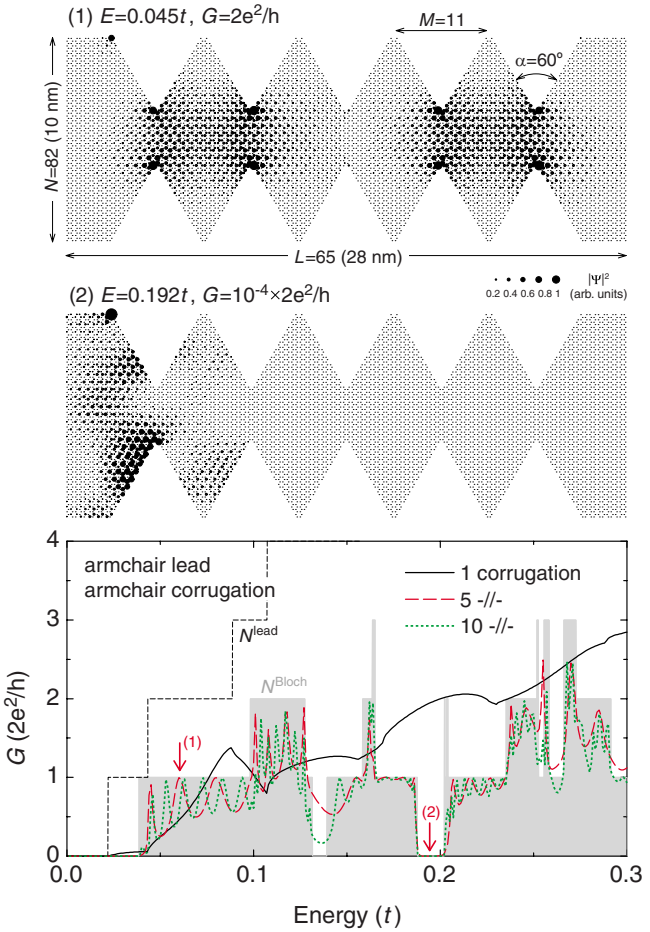

FIG. 5. (Color online) The conductance vs energy for the armchair ribbon with different number of the armchair corrugations. The shaded gray area denotes the number of propagating Bloch states for the periodic corrugation, N^{Bloch}, the same as in Fig. 2(c). The thin black dashed line shows the number of propagating states in the leads, N^{lead}. The top insets present the wave-function modulus for two representative energies marked by arrows for the structure with five corrugations.

corrugations are both armchair. We averaged the conductance over ten realizations of the disorder in order to reduce fluctuations and facilitate visualization of the results. The edge defects act as randomly positioned short-range scatterers and induce strong backscattering. It leads to Anderson localization with substantial transport gaps opened for narrow ribbons.[4,31,32] Even 1% of defects is enough to destroy conductance quantization for the straight ribbon and the Fabry-Perot oscillations for the case of the corrugated ribbon, Fig. 7. The stopbands are smeared already for 5% edge disorder, which indicates that the observation of the miniband formation in the armchair host-corrugated ribbons would require extra-clean, edge-disorder free samples. Note that we also performed calculations for disordered ribbons with the zigzag host. As expected, they showed behavior similar to that shown in Fig. 7 though the defect concentrations producing similar effects on the conductance are significantly larger.

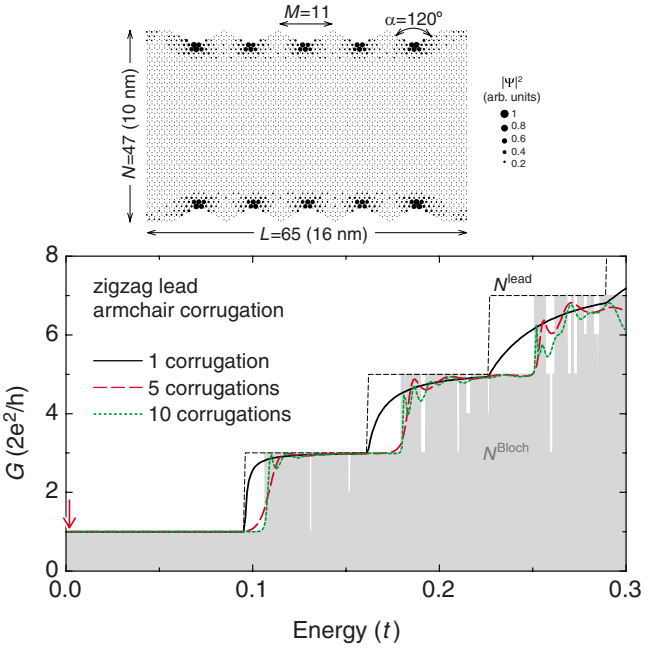

FIG. 6. (Color online) The same as Fig. 5 but for the ribbon with zigzag leads (host).

IV. CONCLUSIONS

We studied the electronic and transport properties of periodic corrugated graphene nanoribbons within the standard p-orbital tight-binding model. We considered both armchair and zigzag underlying host ribbons and three different types of corrugation defined by grooves with armchair edges, zigzag edges, as well as a rectangular corrugation. We calculated the dispersion relations and Bloch states for corrugated ribbons, and demonstrated that they exhibit different features depending on topology of the host ribbon (i.e., armchair or zigzag). For the armchair host, depending on the type of corrugation, a band gap or low-velocity minibands appear near the charge neutrality point $E=0$. For higher energies bands of Bloch states become separated by ministopbands.

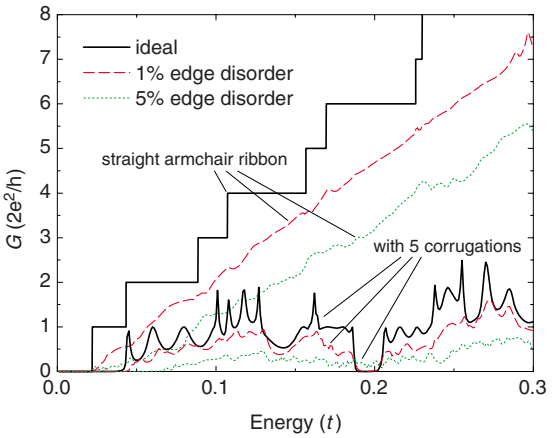

FIG. 7. (Color online) Influence of disorder on the conductance through both the straight armchair ribbon and the ribbon with five armchair corrugations. The structures have the same width $N=82$ (~ 10 nm) and length $L=65$ (~ 28 nm).

By contrast, for corrugated ribbons with the zigzag host, the corrugations introduce neither a band gap nor substantial stopbands (except for the case of the rectangular corrugations).

We calculated the conductance of graphene ribbons with finite numbers of corrugations n. As expected, for sufficiently large n the conductance follows the number of the corresponding propagating Bloch states and shows pronounced oscillations due to the Fabry-Perot interference within the corrugated region. We also argue that for low electron energies the corrugated ribbon with the zigzag host is expected to effectively function as arrays of weakly coupled quantum dots with the conductance dominated by the single-electron charging effects, even though the corrugations can be relatively small in comparison to the ribbon's width.

We also demonstrated that as in the case of uncorrugated ribbons, edge disorder strongly affects the conductance of the corrugated ribbons. Our results indicate that observation of miniband formation in corrugated ribbons would require extra-clean, edge-disorder free samples, especially for the case of the armchair host lattice. Finally, we hope that our study will motivate further experimental investigation of periodically corrugated graphene nanoribbons.

ACKNOWLEDGMENTS

This work was supported by NSERC and the Canadian Institute for Advanced Research. I.V.Z. acknowledges financial support from the Swedish Research Council (VR).

[1] K. S. Novoselov, A. K. Geim, S. V. Morozov, D. Jiang, Y. Zhang, S. V. Dubonos, I. V. Grigorieva, and A. A. Firsov, Science **306**, 666 (2004).
[2] S. Adam, E. H. Hwang, V. Galitski, and S. Das Sarma, Proc. Natl. Acad. Sci. U.S.A. **104**, 18392 (2007).
[3] Z. Chen, Y.-M. Lin, M. J. Rooks, and P. Avouris, Physica E (Amsterdam) **40**, 228 (2007).
[4] M. Y. Han, B. Özyilmaz, Y. Zhang, and P. Kim, Phys. Rev. Lett. **98**, 206805 (2007).
[5] X. Li, X. Wang, L. Zhang, S. Lee, and H. Dai, Science **319**, 1229 (2008).
[6] F. Molitor, A. Jacobsen, C. Stampfer, J. Güttinger, T. Ihn, and K. Ensslin, Phys. Rev. B **79**, 075426 (2009).
[7] F. Miao, S. Wijeratne, Y. Zhang, U. C. Coskun, W. Bao, and C. N. Lau, Science **317**, 1530 (2007).
[8] S. Russo, J. B. Oostinga, D. Wehenkel, H. B. Heersche, S. S. Sobhani, L. M. K. Vandersypen, and A. F. Morpurgo, Phys. Rev. B **77**, 085413 (2008).
[9] C. Stampfer, J. Güttinger, S. Hellmüller, F. Molitor, K. Ensslin, and T. Ihn, Phys. Rev. Lett. **102**, 056403 (2009).
[10] T. Shen, Y. Q. Wu, M. A. Capano, L. P. Rokhinson, L. W. Engel, and P. D. Ye, Appl. Phys. Lett. **93**, 122102 (2008).
[11] X. Jia, M. Hofmann, V. Meunier, B. G. Sumpter, J. Campos-Delgado, J. M. Romo-Herrera, H. Son, Y.-P. Hsieh, A. Reina, J. Kong, M. Terrones, and M. S. Dresselhaus, Science **323**, 1701 (2009).
[12] Ç. Ö. Girit, J. C. Meyer, R. Erni, M. D. Rossell, C. Kisielowski, Li Yang, Ch.-H. Park, M. F. Crommie, M. L. Cohen, S. G. Louie, and A. Zettl, Science **323**, 1705 (2009).
[13] L. P. Kouwenhoven, F. W. J. Hekking, B. J. van Wees, C. J. P. M. Harmans, C. E. Timmering, and C. T. Foxon, Phys. Rev. Lett. **65**, 361 (1990).
[14] M. Leng and C. S. Lent, Phys. Rev. Lett. **71**, 137 (1993).
[15] K. W. Park, S. Lee, M. Shin, J. S. Yuk, E.-H. Lee, and H. C. Kwon, Phys. Rev. B **58**, 3557 (1998).
[16] S. E. Ulloa, E. Castaño, and G. Kirczenow, Phys. Rev. B **41**, 12350 (1990).
[17] Zhi-an Shao, W. Porod, and C. S. Lent, Phys. Rev. B **49**, 7453 (1994).
[18] R. Schuster, K. Ensslin, J. P. Kotthaus, M. Holland, and C. Stanley, Phys. Rev. B **47**, 6843 (1993).
[19] I. V. Zozoulenko, F. A. Maaø, and E. H. Hauge, Phys. Rev. B **53**, 7975 (1996); **53**, 7987 (1996).
[20] T. G. Pedersen, C. Flindt, J. Pedersen, N. A. Mortensen, A. P. Jauho, and K. Pedersen, Phys. Rev. Lett. **100**, 136804 (2008).
[21] Xiaojun Wu and Xiao Cheng Zeng, Nano Res. **1**, 40 (2008).
[22] S. Reich, J. Maultzsch, C. Thomsen, and P. Ordejón, Phys. Rev. B **66**, 035412 (2002); A. H. Castro Neto, F. Guinea, N. M. R. Peres, K. S. Novoselov, and A. K. Geim, Rev. Mod. Phys. **81**, 109 (2009).
[23] Hengyi Xu, T. Heinzel, M. Evaldsson, and I. V. Zozoulenko, Phys. Rev. B **77**, 245401 (2008).
[24] F. Muñoz-Rojas, D. Jacob, J. Fernández-Rossier, and J. J. Palacios, Phys. Rev. B **74**, 195417 (2006).
[25] S. Datta, *Electronic Transport in Mesoscopic Systems* (Cambridge University Press, Cambridge, 1997).
[26] K. Nakada, M. Fujita, G. Dresselhaus, and M. S. Dresselhaus, Phys. Rev. B **54**, 17954 (1996).
[27] M. Ezawa, Phys. Rev. B **73**, 045432 (2006).
[28] H. Benisty, Phys. Rev. B **79**, 155409 (2009).
[29] J. Davies, *The Physics of Low-Dimensional Semiconductors* (Cambridge University Press, Cambridge, 1998).
[30] L. P. Zarbo and B. K. Nikolić, EPL **80**, 47001 (2007).
[31] M. Evaldsson, I. V. Zozoulenko, Hengyi Xu, and T. Heinzel, Phys. Rev. B **78**, 161407(R) (2008).
[32] E. R. Mucciolo, A. H. Castro Neto, and C. H. Lewenkopf, Phys. Rev. B **79**, 075407 (2009).